Journal of the Korean Ceramic Society
Vol. 53, No. 4, pp. 456~462, 2016.

http://dx.doi.org/10.4191/kcers.2016.53.4.456

Microwave Sol-Gel Derived Ho^{3+}/Yb^{3+} Co-Doped $NaCaGd(MoO_4)_3$ Phosphors and their Upconversion Photoluminescence

Chang Sung Lim†

Department of Advanced Materials Science & Engineering, Hanseo University, Seosan 31962, Korea

(Received March 6, 2016; Revised May 19, 2016; Accepted May 25, 2016)

ABSTRACT

$NaCaGd(MoO_4)_3:Ho^{3+}/Yb^{3+}$ ternary molybdates were successfully synthesized by microwave sol-gel method for the first time. Well-crystallized particles formed after heat-treatment at 900°C for 16 h showed a fine and homogeneous morphology with particle sizes of 3-5 μm. Under excitation at 980 nm, the UC intensities of the doped samples exhibited strong yellow emissions based on the combination of strong emission bands at the 520-nm and 630-nm emission bands in the green and red spectral regions, respectively. The strong 520-nm emission band in the green region corresponds to the $^5S_2/^5F_4 \rightarrow {}^5I_8$ transition of Ho^{3+} ions, while the strong 630-nm emission band in the red region appears to be due to the $^5F_5 \rightarrow {}^5I_8$ transition of the Ho^{3+} ions. The optimal Yb^{3+}:Ho^{3+} ratio was found at 9:1, as indicated by the composition-dependent quenching effect of Ho^{3+} ions. The pump power dependence of the upconversion emission intensity and the Commission Internationale de L'Eclairage chromaticity coordinates of the phosphors were evaluated in detail.

Key words : Ternary molybdate, Microwave sol-gel, Yellow phosphors, Upconversion, Raman spectroscopy

1. Introduction

Rare-earth doped oxides based upconversion (UC) particles are receiving extensive interest in recent years due to their stable luminescent properties and potential for application in products such as lasers, three-dimensional displays, light-emitting devices, solar cells, and biological luminescent imaging.[1-3] Previously, scheelite-structured compounds with binary molybdates have been reported to have highly modulated structures due to their unique spectroscopic characteristics and excellent UC photoluminescence properties.[4,5] Rare-earth doped binary $NaLn(MoO_4)_2$ ($Ln = La^{3+}$, Gd^{3+}, Y^{3+}) compounds possess a tetragonal structure and space group $I4_1/a$; they belong to the family of scheelite-type structures. Trivalent rare-earth ions in tetragonal phase can be partially substituted for by Er^{3+}, Ho^{3+}, Tm^{3+}, and Yb^{3+} ions. These ions are effectively doped into the crystal lattices of the tetragonal phase because their radii are similar to those of trivalent rare earth ions; such doping results in the excellent UC photoluminescence properties.[6-8] Among the rare-earth ions, the Ho^{3+} ion, due to its appropriate electronic energy level configuration, is suitable for converting infrared to visible light through the UC process. The Yb^{3+} ion, as a sensitizer, can be dramatically excited by an appropriate incident light source. This energy is transferred to the activator, from which radiation is emitted. The Ho^{3+} ion activator is the luminescence center of the UC particles, while the sensitizer enhances the UC luminescence efficiency. Co-doping of Ho^{3+} and Yb^{3+} ions can remarkably enhance the UC efficiency, allowing a frequency shift from the infrared to the visible range due to the high efficiency of the energy transfer from Yb^{3+} to Ho^{3+}.[9-11]

For the preparation of the binary molybdate $NaLn(MoO_4)_2$, several processes have been developed via specific preparation processes, including solid-state reactions,[12-15] the sol-gel method,[16,17] the Czochralski method,[18-21] the hydrothermal method,[22-26] the microwave assisted hydrothermal method,[27] and the pulse laser deposition.[28] It is necessary to create new ternary molybdate compounds for realization of UC photoluminescence in products with such features as well defined morphology and stable UC luminescent properties. However, no $NaCaGd(MoO_4)_3:Ho^{3+}/Yb^{3+}$ ternary molybdate phosphors have been reported so far. Compared with the usual methods, microwave synthesis has advantages of very short reaction time, small-size particles, narrow particle size distribution, and high purity of final polycrystalline samples. Microwave heating is delivered to the material surface by radiant and/or convection heating, and this heat energy is transferred to the bulk of the material via conduction.[29-31] This is a cost-effective method that can provide products of high homogeneity and can be easily scaled-up; this method is emerging as a viable alternative approach for the quick synthesis of high-quality luminescent materials. In this way, ternary molybdate $NaCaGd(MoO_4)_3:Ho^{3+}/Yb^{3+}$ phosphors synthesized by the microwave sol-gel method are reported for the first time.

In this study, ternary molybdate $NaCaGd_{1-x}(MoO_4)_3:Ho^{3+}/$

†Corresponding author : Chang Sung Lim
E-mail : cslim@hanseo.ac.kr
Tel : +82-41-660-1445 Fax : +82-41-660-1445

Yb^{3+} phosphors with the proper doping concentrations of Ho^{3+} and Yb^{3+} ($x = Ho^{3+} + Yb^{3+}$, $Ho^{3+} = 0.05$, and $Yb^{3+} = 0.35$, 0.40, 0.45, and 0.50) were successfully prepared by the microwave sol-gel method followed by heat treatment. The synthesized particles were characterized by X-ray diffraction (XRD) and scanning electron microscopy (SEM). The pump power dependence of the UC emission intensity and the Commission Internationale de L'Eclairage (CIE) chromatic coordinates were evaluated in detail. The optical properties were examined using photoluminescence (PL) emission and Raman spectroscopy.

2. Experimental Procedure

Stoichiometric amounts of $Ca(NO_3)_2 \cdot 4H_2O$ (99%, Sigma-Aldrich, USA), $Na_2MoO_4 \cdot 2H_2O$ (99%, Sigma-Aldrich, USA), $Gd(NO_3)_3 \cdot 6H_2O$ (99%, Sigma-Aldrich, USA), $(NH_4)_6Mo_7O_{24} \cdot 4H_2O$ (99%, Alfa Aesar, USA), $Ho(NO_3)_3 \cdot 5H_2O$ (99.9%, Sigma-Aldrich, USA), $Yb(NO_3)_3 \cdot 5H_2O$ (99.9%, Sigma-Aldrich, USA), citric acid (99.5%, Daejung Chemicals, Korea), NH_4OH (A.R.), ethylene glycol (A.R.), and distilled water were used to prepare $NaCaGd(MoO_4)_3$, $NaCaGd_{0.6}(MoO_4)_3$: $Ho_{0.05}Yb_{0.35}$, $NaCaGd_{0.55}(MoO_4)_3$: $Ho_{0.05}Yb_{0.40}$, $NaCaGd_{0.50}(MoO_4)_3$: $Ho_{0.05}Yb_{0.45}$, and $NaCaGd_{0.45}(MoO_4)_3$:$Ho_{0.05}Yb_{0.50}$. The compounds $Ca(NO_3)_2$, $Na_2MoO_4 \cdot 2H_2O$, and $(NH_4)_6Mo_7O_{24} \cdot 4H_2O$ were dissolved in 20 mL of ethylene glycol and 80 mL of 5M NH_4OH under vigorous stirring and heating. Subsequently, $Gd(NO_3)_3 \cdot 6H_2O$ with $Ho(NO_3)_3 \cdot 5H_2O$, $Yb(NO_3)_3 \cdot 5H_2O$, and citric acid (with a molar ratio of citric acid to total metal ions of 2:1) were dissolved in 100 mL of distilled water under ibid. Then, the solutions were mixed together vigorously and were heated at 80 - 100°C. Finally, highly transparent solutions were obtained and adjusted to pH = 7 - 8 by the addition of NH_4OH or citric acid. The transparent solutions were placed into a microwave oven operating at a frequency of 2.45 GHz, with maximum output-power of 1250 W for 30 min. The working cycle of the microwave reaction was controlled very precisely using a regime of 40 s on and 20 s off for 15 min; this was followed by further treatment of 30 s on and 30 s off for 15 min. The samples were treated with ultrasonic radiation for 10 min to produce light-yellowish transparent sols. After this, the sols were dried at 120°C in a dry oven to obtain black dried gels. The black dried gels were ground and heat-treated at 900°C for 16 h at 100°C intervals between 600-900°C. Finally, white particles were obtained for pure $NaCaGd(MoO_4)_3$ and pink particles were obtained for the doped compositions.

The crystal structure of the synthesized particles was identified using XRD (D/MAX 2200, Rigaku, Japan). The microstructure and surface morphology of the synthesized particles were observed using SEM (JSM-5600, JEOL, Japan). The PL spectra were recorded using a spectrophotometer (Perkin Elmer LS55, UK) at room temperature. The pump power dependence of the UC emission intensity was measured at levels of working power from 20 to 110 mW. Raman spectra measurements were performed using a LabRam Aramis (Horiba Jobin-Yvon, France) with a spectral resolution of 2 cm^{-1}. The 514.5-nm line of an Ar ion laser was used as an excitation source; the power on the samples was kept at a 0.5 mW level to avoid sample decomposition.

3. Results and Discussion

Figure 1 shows XRD patterns of the (a) JCPDS 29-0351 pattern of powellite $CaMoO_4$, the synthesized (b) pure $NaCaGd(MoO_4)_3$, (c) $NaCaGd_{0.6}(MoO_4)_3$:$Ho_{0.05}Yb_{0.35}$, (d) $NaCaGd_{0.55}(MoO_4)_3$:$Ho_{0.05}Yb_{0.40}$, (e) $NaCaGd_{0.50}(MoO_4)_3$:$Ho_{0.05}Yb_{0.45}$, and (f) $NaCaGd_{0.45}(MoO_4)_3$:$Ho_{0.05}Yb_{0.50}$ particles. In the synthesized samples, almost all XRD peaks can be assigned to the tetragonal phase, which is consistent with the standard data for $CaMoO_4$ (JCPDS 29-0351). The sites of Ca^{2+} or (Na^+/Gd^{3+}) ions were taken as occupied by Ca^{2+}, Na^+, Gd^{3+}, Ho^{3+}, and Yb^{3+} ions at fixed occupation levels as determined by the nominal compositions. The Ho^{3+} and Yb^{3+} ions can be partially doped into the Gd^{3+} sites, so that the Gd^{3+} ions can be efficiently substituted into the Ca^{2+} sites. Consequently, Na^+, Gd^{3+}, Ho^{3+}, and Yb^{3+} ions can be efficiently substituted into the Ca^{2+} sites in the $NaCaGd(MoO_4)_3$ lattice. The ternary undoped and doped $NaCaGd_{1-x}(Ho,Yb)_x(MoO_4)_3$ crystallites provide the strongest intensity peaks from the (112), (204), and (312) planes; these are the major peaks of $CaMoO_4$. Therefore, the synthesized $NaCaGd_{1-x}(MoO_4)_3$ particles belong to the molybdate family and have a scheelite-type structure, with space group $I4_1/a$. It is observed that the diffraction peaks of the ternary undoped and doped $NaCaGd_{1-x}(MoO_4)_3$ samples in Fig. 1(b)-(f) shift slightly to higher angles compared to that of the standard data for $CaMoO_4$ (JCPDS 29-0351) shown in Fig. 1(a). It is well known that the relationship of the interplanar space (d_{hkl}), diffraction angle (θ), and wavelength of X-rays (λ) can be expressed using Bragg's equation:

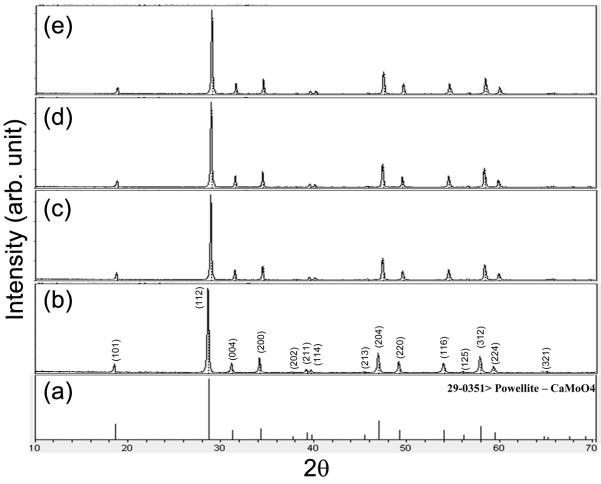

Fig. 1. X-ray diffraction patterns of the (a) JCPDS 29-0351 pattern of $CaMoO_4$, the synthesized (b) pure $NaCaGd(MoO_4)_3$, (c) $NaCaGd_{0.6}(MoO_4)_3$:$Ho_{0.05}Yb_{0.35}$, (d) $NaCaGd_{0.55}(MoO_4)_3$:$Ho_{0.05}Yb_{0.40}$, (e) $NaCaGd_{0.50}(MoO_4)_3$:$Ho_{0.05}Yb_{0.45}$, and (f) $NaCaGd_{0.45}(MoO_4)_3$:$Ho_{0.05}Yb_{0.50}$ particles.

$$2d_{hkl} \sin\theta = \lambda \quad (1)$$

In pure $NaCaGd(MoO_4)_3$ crystals, unit cell decrease occurs due to the substitution of Na^+ (R=1.18 Å) and Gd^{3+} (R=1.053 Å) ions into the Ca^{3+} (R=1.12 Å) sites.[32] According to the Bragg equation (1), the diffraction peaks shift to higher angles with the decrease of the d_{hkl} values. It can also be observed that the diffraction peaks of the doped samples in Fig. 1(c)-(f) shift slightly to higher angles compared to that of the pure $NaCaGd(MoO_4)_3$ sample shown in Fig. 1(b). In the crystal structure of $NaCaGd_{1-x}(MoO_4)_3$, the Gd^{3+} ion site is supposed to be occupied by Ho^{3+} and Yb^{3+} ions with occupations fixed according to the nominal chemical formulas. The defined crystal structure contains MoO_4 tetrahedrons coordinated by four $(Ca/Na/Gd/Ho/Yb)O_8$ square antiprisms through the common O ions. In the doped crystals, unit cell shrinkage results from the substitution of Gd^{3+} ions by Ho^{3+} and Yb^{3+} ions. It is assumed that the radii of Ho^{3+} (R=1.015 Å) and Yb^{3+} (R=0.985 Å) are smaller than that of Gd^{3+} (R=1.053 Å) when the coordination number is CN = 8.[32] Consequently, it should be emphasized that the Ho^{3+} and Yb^{3+} ions can be efficiently doped into the $NaCaGd(MoO_4)_3$ lattice by partial substitution of Ho^{3+} and Yb^{3+} for Gd^{3+} in the Gd^{3+} sites, which leads to unit cell shrinkage while the tetragonal structure of $NaCaGd_{1-x}(Ho,Yb)_x(MoO_4)_3$ maintains. Post heat-treatment plays an important role in establishing a well-defined crystallized morphology. To reach a well-defined final morphology, the samples need to be heat treated at 900°C for 16 h. It is assumed that the Ho^{3+}/Yb^{3+} doping concentrations are acceptable to keep the original structure of $NaCaGd(MoO_4)_3$.

Figure 2 provides SEM images of the synthesized (a) $NaCaGd_{0.6}(MoO_4)_3:Ho_{0.05}Yb_{0.35}$ and (b) $NaCaGd_{0.50}(MoO_4)_3:Ho_{0.05}Yb_{0.45}$ particles. The as-synthesized samples are well crystallized, with a fine and homogeneous morphology and a particle size of 3-5 μm. The samples show no discrepancy in terms of morphological features, and agglomerated particles are induced by atom inter-diffusion between the grains. It should be noted that the morphological feature is insensitive to the Ho^{3+}/Yb^{3+} doping concentration. The microwave sol-gel method in application to ternary molybdates provides the energy to synthesize the bulk of the material uniformly, so that fine particles with controlled morphology can be fabricated in a short time period. This method is a cost-effective way to fabricate highly homogeneous products with easy scale-up; it is a viable alternative to the rapid synthesis of UC particles. This suggests that the microwave sol-gel route is suitable for the creation of homogeneous $NaCaGd_{1-x}(MoO_4)_3:Ho^{3+}/Yb^{3+}$ crystallites.

Figure 3 shows UC photoluminescence emission spectra of the as-prepared (a) $NaCaGd_{0.6}(MoO_4)_3:Ho_{0.05}Yb_{0.35}$, (b) $NaCaGd_{0.55}(MoO_4)_3:Ho_{0.05}Yb_{0.40}$, (c) $NaCaGd_{0.50}(MoO_4)_3:Ho_{0.05}Yb_{0.45}$, and (d) $NaCaGd_{0.45}(MoO_4)_3:Ho_{0.05}Yb_{0.50}$ excited under 980 nm at room temperature. The UC particles exhibited yellow emissions based on a strong 520 nm emission band in the green region and a strong 630-nm emission band in the red region. The UC intensity of (c) $NaCaGd_{0.50}(MoO_4)_3:Ho_{0.05}Yb_{0.45}$ is the highest of all particles. The strong 520-nm emission band in the green region corresponds to the $^5S_2/^5F_4 \rightarrow {}^5I_8$ transition, while the very strong 630-nm emission band in the red region corresponds to the $^5F_5 \rightarrow {}^5I_8$ transition to the activator, where radiation is emitted. The Ho^{3+} ion activator is the luminescence center for these UC particles; the sensitizer Yb^{3+} effectively enhances the UC luminescence intensity because of the efficient energy transfer from Yb^{3+} to Ho^{3+}. As can be seen in Fig. 3, the highest intensity of (c) $NaCaGd_{0.50}(MoO_4)_3:Ho_{0.05}Yb_{0.45}$ resulted for the ratio of Yb^{3+}: Ho^{3+} 9:1, while the lowest intensity of (a) $NaCaGd_{0.6}(MoO_4)_3$: $Ho_{0.05}Yb_{0.35}$ for the ratio of Yb^{3+}:Ho^{3+} 7 : 1. The optimal Yb^{3+}:Ho^{3+} ratio 9 : 1 is induced by the concentration quenching effect of the Ho^{3+} ion. Therefore, the higher content of the Yb^{3+} ion, used as a sensitizer, and the lower content of the Ho^{3+} ion, used to ensure the correct ratio of Yb^{3+}:Ho^{3+} (9 : 1), can remarkably enhance the UC luminescence through efficient energy transfer. The concentration quenching effect can be explained by the energy transfer between nearest Ho^{3+} and Yb^{3+} ions. With the increase of the Ho^{3+} and Yb^{3+} ion concentrations, the distance between Ho^{3+} and Yb^{3+} ions decreases, which can promote non-radiative

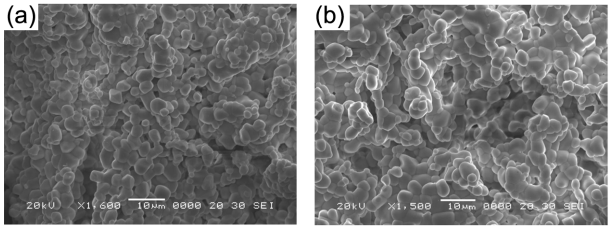

Fig. 2. Scanning electron microscopy images of the synthesized (a) $NaCaGd_{0.6}(MoO_4)_3:Ho_{0.05}Yb_{0.35}$ and (b) $NaCaGd_{0.50}(MoO_4)_3:Ho_{0.05}Yb_{0.45}$ particles.

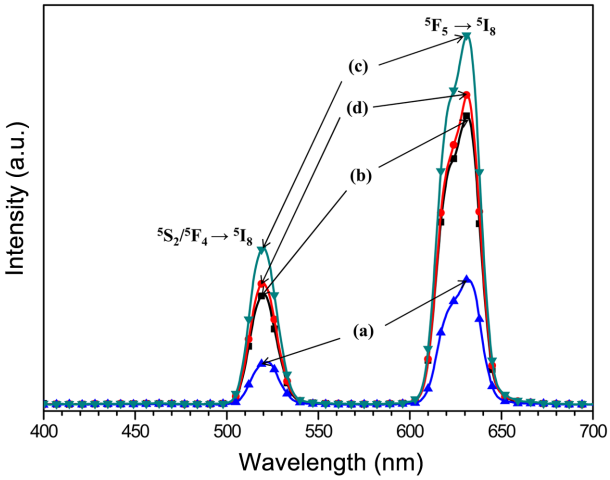

Fig. 3. Upconversion photoluminescence emission spectra of (a) $NaCaGd_{0.6}(MoO_4)_3:Ho_{0.05}Yb_{0.35}$, (b) $NaCaGd_{0.55}(MoO_4)_3:Ho_{0.05}Yb_{0.40}$, (c) $NaCaGd_{0.50}(MoO_4)_3:Ho_{0.05}Yb_{0.45}$, and (d) $NaCaGd_{0.45}(MoO_4)_3:Ho_{0.05}Yb_{0.50}$ excited under 980 nm at room temperature.

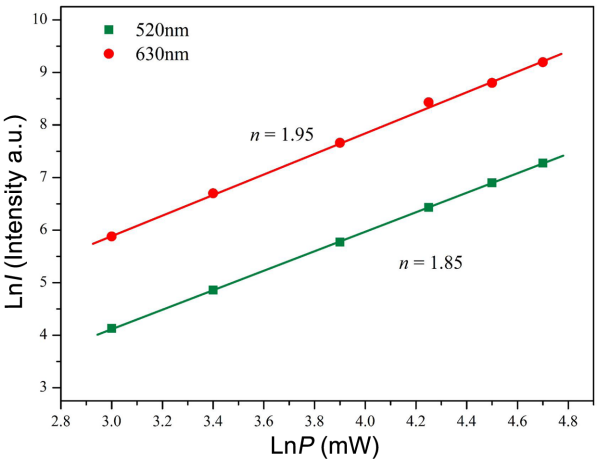

Fig. 4. Logarithmic scale dependence of the upconversion emission intensity on the pump power in the range of 20 to 110 mW at 520 and 630 nm in the $NaCaGd_{0.50}(MoO_4)_3:Ho_{0.05}Yb_{0.45}$ sample.

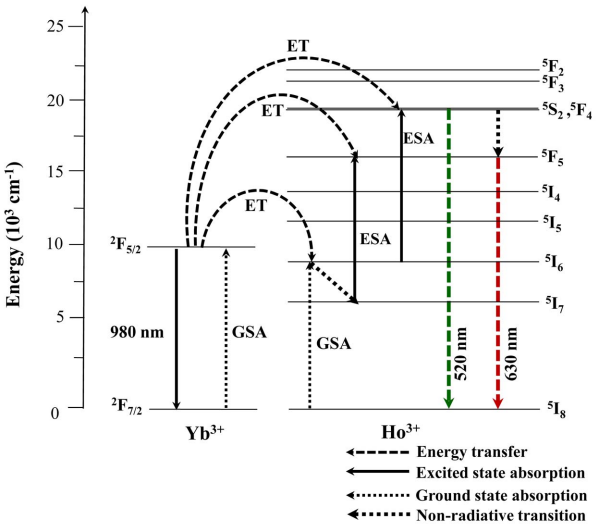

Fig. 5. Schematic energy level diagrams of Yb^{3+} (sensitizer) and Er^{3+} (activator) ions in the $NaCaGd_{1-x}(MoO_4)_3:Ho^{3+}/Yb^{3+}$ system and the upconversion mechanisms of the green and red emissions under 980 nm laser excitation.

energy transfer via an exchange interaction or multipole-multipole interactions.[33]

The logarithmic scale dependence of the UC emission intensities at 520 and 630 nm on the working pump power over the range of 20 to 110 mW in the $NaCaGd_{0.50}(MoO_4)_3:Ho_{0.05}Yb_{0.45}$ sample is shown in Fig. 4. In the UC process, the UC emission intensity is proportional to the slope value n of the irradiation pumping power, where n is the number of pumped photons required to produce UC emission:[34]

$$I \propto P^n \quad (2)$$

$$\mathrm{Ln}I \propto n\mathrm{Ln}P \quad (3)$$

where the value n is the number of pumped photons required to excite the upper emitting state, I is the UC luminescent intensity, and P is the laser pumping power. As is evident in Fig. 4, the slope value calculations indicate a value of $n = 1.95$ for the red emission at 630 nm, and a value of $n = 1.85$ for the green emission at 520 nm. These results show that the UC mechanism of the green and red emissions can be explained by a two-photon UC process in Ho^{+3}/Yb^{3+} co-doped phosphors.[4,9-12]

Based on the results of pump power dependence, the known schematic energy level diagrams of Ho^{3+} (activator) and Yb^{3+} (sensitizer) ions in the as-prepared $NaCaGd_{1-x}(MoO_4)_3:Ho^{3+}/Yb^{3+}$ samples, and the UC mechanisms, which account for the green and red emissions during 980 nm laser excitation, are shown in Fig. 5. The UC emissions are generated by a two photon process through excited state absorption (ESA) and energy transfer (ET).[4,10,12] Initially, the Yb^{3+} ion sensitizer is excited from the $^2F_{7/2}$ level to the $^2F_{5/2}$ level under excitation by 980 nm pumping; the Yb^{3+} ion sensitizer transfers its energy to the Ho^{3+} ions. Then, the Ho^{3+} ions are populated from the $^5I_8$ ground state to the $^5I_6$ excited state. This is a phonon-assisted energy transfer process because of the energy mismatch between the $^2F_{5/2}$ level of Yb^{3+} and the $^5I_6$ level of Ho^{3+}. Second, the Ho^{3+} in the $^5I_6$ level is excited to the $^5S_2$ or $^5F_4$ level by the next energy transfer from Yb^{3+}. In addition, the $^5S_2/^5F_4$ level of Ho^{3+} can be populated through excited state absorption. Finally, the green emission around 520 nm, corresponding to the $^5S_2/^5F_4 \rightarrow {}^5I_8$ transition, takes place. For the red emission, the population of the $^5F_5$ level is generated by two different channels. In one channel, the Ho^{3+} in the $^5S_2/^5F_4$ level state relaxes non-radiatively to the $^5F_5$ level. Another channel is closely related to the $^5I_7$ level, populated by non-radiative relaxation from the $^5I_6$ excited state. The Ho^{3+} in the $^5I_7$ level is excited to the $^5F_5$ level by energy transfer from Yb^{3+} and relaxes to the $^5F_5$ level. Therefore, the red emission around 630 nm corresponds to the $^5F_5 \rightarrow {}^5I_8$ transition.[35,36]

In Fig. 6, (A) calculated chromaticity coordinates (x, y) and (B) a CIE chromaticity diagram are shown for the compositions (a) $NaCaGd_{0.6}(MoO_4)_3:Ho_{0.05}Yb_{0.35}$, (b) $NaCaGd_{0.55}(MoO_4)_3:Ho_{0.05}Yb_{0.40}$, (c) $NaCaGd_{0.50}(MoO_4)_3:Ho_{0.05}Yb_{0.45}$, and (d) $NaCaGd_{0.45}(MoO_4)_3:Ho_{0.05}Yb_{0.50}$. The triangle in Fig. 6(B) indicates standard coordinates for blue, green, and red colors. The inset in Fig. 6(B) shows the chromaticity points for the samples (a), (b), (c), and (d). The chromaticity coordinates (x, y) are strongly dependent on the Ho^{3+}/Yb^{3+} concentration ratio. As can be seen in Fig. 6(A), the calculated chromaticity coordinates x = 0.413 and y = 0.376 for (a) $NaCaGd_{0.6}(MoO_4)_3:Ho_{0.05}Yb_{0.35}$, the values of x = 0.447 and y = 0.388 for (b) $NaCaGd_{0.55}(MoO_4)_3:Ho_{0.05}Yb_{0.40}$, the values of x = 0.462 and y = 0.397 for (c) $NaCaGd_{0.50}(MoO_4)_3:Ho_{0.05}Yb_{0.45}$, and the values of x = 0.472 and y = 0.402 for (d) $NaCaGd_{0.45}(MoO_4)_3:Ho_{0.05}Yb_{0.50}$ correspond to the standard equal energy points in the CIE diagram shown in Fig. 6(B).

Figure 7 shows the Raman spectra of the synthesized (a) pure

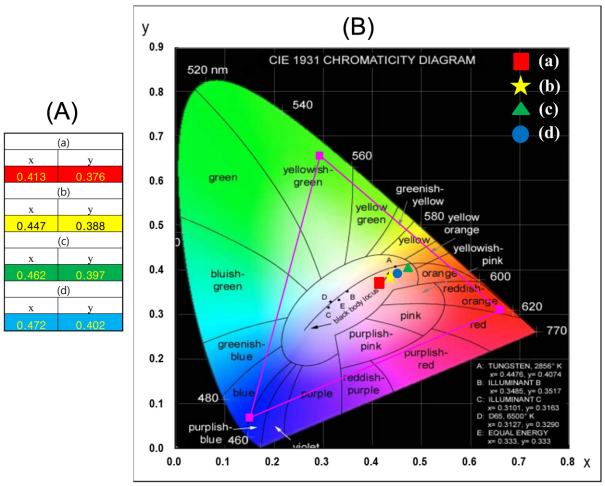

Fig. 6. (A) Calculated chromaticity coordinate (x, y) values and (B) CIE chromaticity diagram for $NaCaGd_{1-x}(MoO_4)_3:Ho^{3+}/Yb^{3+}$ phosphors. The inset shows the emission points for the samples synthesized with (a) $NaCaGd_{0.6}(MoO_4)_3:Ho_{0.05}Yb_{0.35}$, (b) $NaCaGd_{0.55}(MoO_4)_3:Ho_{0.05}Yb_{0.40}$, (c) $NaCaGd_{0.50}(MoO_4)_3:Ho_{0.05}Yb_{0.45}$, and (d) $NaCaGd_{0.45}(MoO_4)_3:Ho_{0.05}Yb_{0.50}$ particles.

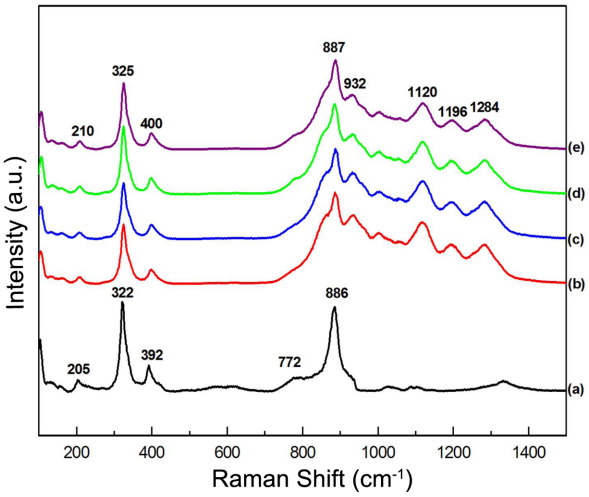

Fig. 7. Raman spectra of the synthesized (a) pure $NaCaGd(MoO_4)_3$, (b) $NaCaGd_{0.6}(MoO_4)_3:Ho_{0.05}Yb_{0.35}$, (c) $NaCaGd_{0.55}(MoO_4)_3:Ho_{0.05}Yb_{0.40}$, (d) $NaCaGd_{0.50}(MoO_4)_3:Ho_{0.05}Yb_{0.45}$, and (e) $NaCaGd_{0.45}(MoO_4)_3:Ho_{0.05}Yb_{0.50}$ particles excited by the 514.5-nm line of an Ar ion laser at 0.5 mW.

$NaCaGd(MoO_4)_3$, (b) $NaCaGd_{0.6}(MoO_4)_3:Ho_{0.05}Yb_{0.35}$, (c) $NaCaGd_{0.55}(MoO_4)_3:Ho_{0.05}Yb_{0.40}$, (d) $NaCaGd_{0.50}(MoO_4)_3:Ho_{0.05}Yb_{0.45}$, and (e) $NaCaGd_{0.45}(MoO_4)_3:Ho_{0.05}Yb_{0.50}$ particles excited by the 514.5-nm line of an Ar ion laser at 0.5 mW. The internal modes for the (a) pure $NaCaGd(MoO_4)_3$ particles were detected at 126, 205, 322, 392, 772, and 886 cm^{-1}. The well-resolved sharp peaks for $NaCaGd(MoO_4)_3$ indicate the high crystallinity of the synthesized particles. The internal vibration mode frequencies are dependent on the lattice parameters and on the strength of the partially covalent bond between the cation and the molecular ionic group MoO_4. The Raman spectrum of the $NaCaGd(MoO_4)_3$ crystal in Fig. 7(a) is that of the typical molybdate compounds, and is divided into two parts, with a wide empty gap of 400-750 cm^{-1}.[4,37,38] The highest intensity of the wavenumber band at 886 cm^{-1} corresponds to stretching vibrations of MoO_4. Stretching vibrations of the Mo-O bonds are observed in the 772 cm^{-1} region. For these stretching vibrations, strong mixing occurs between the Mo-O bonds and the MoO_4. The bands at 322 and 392 cm^{-1} may have originated from vibrations of the longer Mo-O bonds, which are employed in the formation of the Mo-Mo bridge. Translational vibration motion of the Ca^{3+} ions is observed at 205 cm^{-1}, whereas the Gd^{3+} translations are located below 180 cm^{-1}.[39,40] The Raman spectra of the doped particles indicate the presence of highly modulated peaks at higher frequencies of 887, 932, 1120, 1196, and 1284 cm^{-1} and at lower frequencies of 210, 325, and 400 cm^{-1}. It should be emphasized that these strong modulated peaks of the doped samples recorded under excitation at 514.5 nm are superimposed due to strong Ho^{3+} luminescence lines and strongly affected by the concentration quenching effect of Ho^{3+} ions.[41,42] These results lead to high emitting efficiency; the involved materials can be considered as potential active components in new optoelectronic devices and biomedical applications.

4. Conclusions

Ternary molybdate $NaCaGd(MoO_4)_3:Ho^{3+}/Yb^{3+}$ phosphors were successfully synthesized by microwave sol-gel method. Well-crystallized particles formed after heat-treatment at 900°C for 16 h showed fine and homogeneous morphology, with particle sizes of 3 - 5 μm. Under excitation at 980 nm, the doped $NaCaGd_{1-x}(MoO_4)_3:Ho^{3+}/Yb^{3+}$ particles exhibited yellow emissions based on a strong 520-nm emission band in the green region and a very strong 630-nm emission band in the red region; these emissions were assigned to the $^5S_2/^5F_4 \rightarrow {}^5I_8$ and $^5F_5 \rightarrow {}^5I_8$ transitions, respectively. The optimal $Yb^{3+}:Ho^{3+}$ ratio was found at 9 : 1, and was determined to be controlled by the concentration quenching effect of the Ho^{3+} ion. The slope value calculations indicate a value of $n = 1.95$ for the red emission at 630 nm, and a value of $n = 1.85$ for the green emission at 520 nm. The calculated chromaticity coordinates were found to correspond to the standard equal energy point in the CIE diagram. The highly modulated Raman spectra of the doped samples, recorded under excitation at 514.5 nm, were superimposed due to strong Ho^{3+} luminescence lines and strongly affected by the concentration quenching effect of Ho^{3+} ions. These results can be considered as indicating that these materials have the potential for use as active components in new optoelectronic devices and biomedical applications.

Acknowledgments

This research was supported by the Basic Science Research

Program through the National Research Foundation of Korea (NRF), funded by the Ministry of Education (2015-058813).

REFERENCES

1. M. Lin, Y. Zho, S. Wang, M, Liu, Z. Duan, Y. Chen, F. Li, F. Xu, and T. Lu, "Recent Advances in Synthesis and Surface Modification of Lanthanide-Doped Upconversion Nanoparticles for Biomedical Napplications," *Biotechnol. Adv.*, **30** [6] 1551-61 (2012).
2. M. V. DaCosta, S. Doughan, and U. J. Krull, "Lanthanide Upconversion Nanoparticles and Application in Bioassays and Bioimaging: A Review," *Anal. Chim. Acta*, **832** [1] 1-33 (2014).
3. M. Wang, G. Abbineni, A. Clevenger, C. Mao, and S. Xu, "Upconversion Nanoparticles: Synthesis, Surface Modification and Biological Applications," *Nanomed.: Nanotech. Biol. Med.*, **7** [6] 710-29 (2011).
4. C. S. Lim, A. Aleksandrovsky, M. Molokeev, A. Oreshonkov, and V. Atuchin, "The Modulated Structure and Frequency Upconversion Properties of $CaLa_2(MoO_4)_4$:Ho^{3+}/Yb^{3+} Phosphors Prepared by Microwave Synthesis," *Phys. Chem. Chem. Phys.*, **17** [9] 19278-87 (2015).
5. C. S. Lim, "Highly Modulated Structure and Upconversion Photoluminescence Properties of $PbGd_2(MoO_4)_4$:Er^{3+}/Yb^{3+} Phosphors," *Mater. Res. Bull.*, **75** [3] 211-16 (2016).
6. J. Liao, D. Zhou, B. Yang, R. Liu, Q. Zhang, and Q. Zhou, "Sol-Gel Preparation and Photoluminsence Properties of $CaLa_2(MoO_4)_4$:Eu^{3+} Phosphors," *J. Lumin.*, **134** [6] 533-38 (2013).
7. J. Sun, Y. Lan, Z. Xia, and H. Du, "Sol-Gel Synthesis and Green Upconversion Luminescence in $BaGd_2(MoO_4)_4$:Yb^{3+}, Er^{3+} Phosphors," *Opt. Mater.*, **33** [6] 576-81 (2011).
8. C. Guo, H. K. Yang, and J. H. Jeong, "Preparation and Luminescence Properties of Phosphor $MGd_2(MoO_4)_4$:Eu^{3+} (M=Ca, Sr and Ba)," *J. Lumin.*, **130** [11] 1390-93 (2010).
9. Z. Shan, D. Chen, Y. Yu, P. Huang, F. Weng, H. Lin, and Y. Wang, "Upconversion Luminescence of Ho^{3+} Sensitized by Yb^{3+} in Transparent Glass Ceramic Embedding $BaYF_5$ Nanocrystals," *Mater. Res. Bull.*, **45** [8] 1017-20 (2010).
10. W. Liu, J. Sun, X. Li, J. Zhang, Y. Tian, S. Fu, H. Zhong, T. Liu, L. Cheng, H. Xia, B. Dong, R. Hua, X. Zhang, and B. Chen, "Laser Induced Thermal Effect on Upconversion Luminescence and Temperature-Dependent Upconversion Mechanism in Ho^{3+}/Yb^{3+}-Codoped $Gd_2(WO_4)_3$ Phosphor," *Opt. Mater.*, **35** [7] 1487-92 (2013).
11. W. Xu, H. Zhao, Y. Li, L. Zheng, Z. Zhang, and W. Cao, "Optical Temperature Sensing through the Upconversion Luminescence from Ho^3+/Yb^{3+} Codoped $CaWO_4$," *Sens. Actuators, B*, **188** [9] 1096-100 (2013).
12. J. Tang, C. Cheng, Y. Chen, and Y. Huang, "Yellow-Green Upconversion Photoluminescence in Yb^{3+}, Ho^{3+} Co-Doped $NaLa(MoO_4)_2$ Phosphor," *J. Alloys Compd.*, **609** [3] 268-73 (2014).
13. W. Zhang, J. Li, Y. Wang, J. Long, and K. Qiu, "Synthesis and Luminescence Properties of $NaLa(MoO_4)_{2-x}AG_x$:Eu^{3+} ($AG=SO_4^{2-}$, BO_3^{3-}) Red Phosphors for White Light Emitting Diodes," *J. Alloys Compd.*, **635** [1] 16-20 (2015).
14. F. Mo, L. Zhou, Q. Pang, F. Gong, and Z. Liang, "Potential Red-Emitting $NaGd(MoO_4)_2$:R (M=W, Mo, R=Eu^{3+}, Sm^{3+}, Bi^{3+}) Phoshors for White Light Emitting Diodes Applications," *Ceram. Int.,* **38** [9] 6289-94 (2012).
15. G. Li, S. Lan, L. Li, M. Li, W. Bao, H. Zou, X. Xu, and S. Gan, "Tunable Luminescence Properties of $NaLa(MoO_4)_2$: Ce^{3+},Tb^{3+} Phosphors for near UV-Excited White Light-Emitting-Diodes," *J. Alloys Compd.*, **513** [2] 145-49 (2012).
16. J. Liao, H. Huang, H. You, X. Qiu, Y. Li, B. Qui, and H.-R. Wen, "Photoluminescence Properties of $NAGd(MoO_4)_2$:Eu^{3+} Nanophosphors Prepared by Sol-Gel Method," *Mater. Res. Bull.*, **45** [10] 1145-49 (2010).
17. F. Cao, L. Li, Y. Tian, and X. Wu, "Sol-Gel Synthesis of Red Emitting $[Na_{0.6}La_{0.8-x}Eu_x]_2(MoO_4)_3$ Phosphors and Improvement of its Luminescent Properties by the Co-Doping Method," *Opt. Laser Technol.*, **55** [1] 6-10 (2014).
18. G. M. Kuz'micheva, D. A. Lis, K. A. Subbotin, V. B. Rybakov, and E. V. Zharikov, "Growth and Structural X-ray Investigations of Scheelite-like Single Crystals Er, Ce: $NaLa(MoO_4)_2$ and Yb:$NaGd(WO_4)_2$," *J. Cryst. Growth*, **275** [12] e1835-42 (2005).
19. X. Lu, Z. You, J. Li, Z. Zhu, G. Jia, B. Wu, and C. Tu, "Optical Absortion and Spectroscopic Characteristics of Tm^{3+} Ions Doped $NaY(MoO_4)_2$ Crystal," *J. Alloys Compd.*, **458** [5] 462-66 (2008).
20. X. Li, Z. Lin, L. Zhang, and G. Wang, "Growth, Thermal and Spectral Properties of Nd^{3+}-Doped $NaGd(MoO_4)_2$ Crystal," *J. Cryst. Growth*, **290** [7] 670-73 (2006).
21. Y. K.Voron'ko, K.A. Subbotin, V. E. Shukshin, D. A. Lis, S. N. Ushakov, A. V. Popov, and E. V. Zharikov, "Growth and Spectroscopic Investigations Yb^{3+}-Doped $NaGd(MoO_4)_2$ and $NaLa(MoO_4)_2$ - New Promising Laser Crystals," *Opt. Mater.*, **29** [3] 246-52 (2009).
22. H. Lin, X. Yan, and X. Wang, "Controllable Synthesis and Down-Conversion Properties of Flower-like $NaY(MoO_4)_2$ Microcrystals via Polyvinylpyrrolidone-Mediateds," *J. Solid State Chem.*, **204** [3] 266-71 (2013).
23. G. Li, L. Li, M. Li, W. Bao, Y. Song, S. Gan, H. Zou, and X. Xu, "Hydrothermal Synthrsis and Luminescence Properties of $NaLa(MoO_4)_2$:Eu^{3+},Tb^{3+} Phosphors," *J. Alloys Compd.,* **550** [1] 1-8 (2013).
24. Y. Huang, L. Zhou, L. Yang, and Z. Tang, "Self-Assembled 3D Flower-like $NaY(MoO_4)_2$:Eu^{3+} Microarchitectures: Hydrothermal Synthesis, Formation Mechanism and Luminescence Properties," *Opt. Mater.*, **33** [8] 777-82 (2011).
25. L. Li, W. Zi, G. Li, S. Lan, G. Ji, S. Gan, H. Zou, and X. Xu, "Hydrothermal Synthesis and Luminescent Properties of $NaLa(MoO_4)_2$:Dy^{3+} Phorsphor," *J. Solid State Chem.*, **191** [2] 175-80 (2012).
26. Y. Tian, B. Chen, B. Tian, J. Sun, X. Li, J. Zhang, L. Cheng, H. Zhong, Q. Meng, and R. Hua, "Ionic Liquid-Assisted Hydrothermal Synthesis of Dendrite-like $NaY(MoO_4)_2$:Tb^{3+} Phosphor," *Phys. B*, **407** [8] 2556-59 (2012).
27. J. Zhang, X. Wang, X. Zhang, X. Zhao, X. Liu, and L. Peng, "Microwave Synthesis of $NaLa(MoO_4)_2$ Microcrystals and their Near-Infrared Luminescent Properties with Lathanide Ion Doping (Er^{3+}, Nd^{3+}, Yb^{3+})," *Inorg. Chem. Commun.*, **14** [9] 1723-27 (2011).
28. S. W. Park, B. K. Moon, B. C. Choi, J. H. Jeong, J. S. Bae,

and K. H. Kim, "Red Photoluminescence of Pulsed Laser Deposited Eu:NaY(MoO_4)$_2$ Thin Film Phosphors on Sapphire Substrates," *Curr. Appl. Phys.*, **12** [12] S150-55 (2012).
29. C. S. Lim, "Cyclic MAM Synthesis and Upconversion Photoluminescence Properties of $CaMoO_4$:Er^{3+}/Yb^{3+} Particles," *Mater. Res. Bull.*, **47** [1] 4220-25 (2012).
30. C. S. Lim, "Microwave-Assisted Synthesis of $CdWO_4$ by Solid-State Metathetic Reaction," *Mater. Chem. Phys.*, **131** [8] 714-18 (2012).
31. C. S. Lim, "Upconversion Photoluminescence Properties of $SrY_2(MoO_4)_4$:Er^{3+}/Yb^{3+} Phosphors Synthesized by a Cyclic Microwave-Modified Sol-Gel Method," *Infrared Phys. Technol.*, **67** [4] 371-76 (2014).
32. R. D. Shannon, "Revised Effective Ionic Radii and Systematic Studies of Interatomic Distances in Halides and Chalcogenides," *Acta Crystallogr., Sect. A: Cryst. Phys., Diffr., Theor. Gen. Crystallogr.*, **A32** [8] 751-67(1976).
33 F. Anzel, G. Baldacchini, L. Laversenne, and G. Boulon, "Radiation Trapping and Self-Quenching Analysis in Yb^{3+}, Er^{3+}, and Ho^{3+} Doped Y_2O_3," *Opt. Mat.*, **24** [2] 103-9 (2003).
34. H. Guo, N. Dong, M. Yin, W. Zhang, L. Lou, and S. Xia, "Visible Upconversion in Rare Earth-Doped Gd_2O_3 Nanocrystals," *J. Phys. Chem. B,* **108** [7] 19205-9 (2004).
35. Y. Xu, Y. Wang, L. Shi, L. Xing, and X. Tan, "Bright White Upconversion Luminescence in Ho^{3+}/Yb^{3+}/Tm^{3+} Triple Doped $CaWO_4$ Polycrystals," *Opt. Laser Technol.*, **54** [1] 50-2 (2013).
36. X. Li, Q. Nie, S. Dai, T. Xu, L. Lu, and X. Zhang, "Energy Transfer and Frequency Upconversion in Ho^{3+}/Yb^{3+} Co-Doped Bismuth-Germanate Glasses," *J. Alloys Compd.*, **454** [6] 510-14 (2008).
37. V. V. Atuchin, V. G. Grossman, S. V. Adichtchev, N. V. Surovtsev, T. A. Gavrilova, and B. G. Bazarov, "Structural and Vibrational Properties of Microcrystalline TIM(MoO_4)$_2$ (M = Nd, Pr) Molybdates," *Opt. Mater.*, **34** [9] 812-16 (2012).
38. A. A. Savina, V. V. Atuchin, S. F. Solodovnikov, Z. A. Solodovnikova, A. S. Krylov, E. A. Maximovskiy, M. S. Molokeev, A. S. Oreshonkov, A. M. Pugachev, and E. G. Khaikina, "Synthesis, Structural and Spectroscopic Properties of Acentric Triple Molybdate $Cs_2NaBi(MoO_4)_3$," *J. Solid State Chem.*, **225** [1] 53-8 (2015).
39. V. V. Atuchin, O. D. Chimitova, T. A. Gavrilova, M. S. Molokeev, S.-J. Kim, N. V. Surovtsev, and B. G. Bazarov, "Synthesis, Structural and Vibration Properties of Microcrysyalline $RbNd(MoO_4)_2$," *J. Cryst. Growth,* **318** [7] 683-86 (2011).
40. V. V. Atuchin, O. D. Chimitova, S. V. Adichtchev, J. G. Bazarov, T. A. Gavrilova, M. S. Molokeev, N. V. Surovtsev, and Z. G. Bazarova, "Synthesis, Structural and Vibration Properties of Microcrysyalline ß-$RbSm(MoO_4)_2$," *Mater. Lett.,* **106** [1] 26-9 (2013).
41. C. S. Lim, A. Aleksandrovsky, M. Molokeev, A. Oreshonkov, and V. Atuchin, "Microwave Sol-Gel Synthesis and Upconversion Photoluminescence Properties of $CaGd_2(WO_4)_4$:Er^{3+}/Yb^{3+} Phosphors with Incommensurately Modulated Structure," *J. Solid State Chem.*, **228** [2] 160-66 (2015).
42. C. S. Lim, "Microwave Sol-Gel Derived $NaCaGd(MoO_4)_3$: Er^{3+}/Yb^{3+} Phosphors and their Upconversion Photoluminescence Pproperties," *Infrared Phys. Technol.*, **76** [3] 353-59 (2016).